ELSEVIER

Mapping Deforestation and Secondary Growth in Rondonia, Brazil, Using Imaging Radar and Thematic Mapper Data

Eric Rignot,† *William A. Salas,** *and David L. Skole**

Excellent data on deforestation have been obtained in the tropics with the use of high-resolution optical sensors. Yet, several problems remain. Cloud cover creates data gaps that limit the possibility of complete and frequent assessments, and secondary growth is not well characterized. Active microwave sensors could complement these sensors because they operate independently of cloud cover and smoke and can detect differences in woody biomass and forest structure associated with various stages of forest clearing and regrowth. An example of comparison and synergy between the two techniques is discussed here. Polarimetric, C- (5.6 cm) and L-band (24 cm) frequency, radar data gathered in October 1994 by NASA's Spaceborne Imaging Radar C, on a test site southeast of the city of Porto Velho, in the state of Rondonia, Brazil, are analyzed in conjunction with one 1993 Landsat Thematic Mapper (TM) scene, a 9-year time series of Satellite pour l'observation de la Terre (SPOT) XS data, two Japan Earth Resources Satellite (JERS-1) radar images from 1994 and 1995, and a field visit conducted in 1995.

The C-band radar data are found to be of limited utility for mapping deforestation. At L-band, multiple polarizations are required to obtain a reliable classification. The single polarization, L-band, single date, JERS-1 data underestimate the extent of deforestation, especially during the wet season. With multiple polarizations, six classes of land cover, including one level of regrowth, are mapped with 90% accuracy, but intermediate regrowth 5–8 years of age is not well separated from the forest. The Landsat TM data identify deforested areas better but provide less information on residual woody biomass levels. Combining the two classifications, seven classes of land cover including two levels of regrowth are mapped with 93% accuracy. The results show that the deforestation rate for 1994 was 1.7%. Large variations in residual woody biomass are detected among new clearings. Half of the total deforested land is in some stage of regrowth, but most of it is less than 5 years old. Secondary growth is therefore a significant form of land use that is recleared quickly. ©Elsevier Science Inc., 1997.

INTRODUCTION

In the past two centuries, the concentration of atmospheric carbon dioxide has increased by >25% (Neftel et al., 1985). Most of the current flux is attributed to fossil fuel burning, but a third is thought to have come from deforestation in the tropics (Houghton, 1991; Houghton and Skole, 1990; Houghton et al., 1991). Although it is generally agreed that tropical land-use change is a net source of atmospheric carbon, estimating the magnitude of this source is difficult. Three types of data are required to calculate its magnitude: (1) the rates and geographic distribution of deforestation; (2) the fate of deforested land, including regrowth and reclearing; and (3) the changes in the stocks of carbon above and below ground as a result of disturbance and recovery time. Although the rate and extent of deforestation have become more accurately documented in recent years, large uncertainties remain in the estimates of carbon stocks in soil and vegetation (Houghton, 1991) and in the fate of deforested land (Skole et al., 1994).

Satellite remote sensing has helped quantity defores-

* Institute for the Study of Earth, Oceans, and Space, University of New Hampshire, Durham

† Jet Propulsion Laboratory, California Institute of Technology, Pasadena

Address correspondence to Eric Rignot, Jet Propulsion Laboratory, California Institute of Technology, 4800 Oak Grove Drive, Pasadena, CA 91109-8099.

Received 19 February 1996; revised 13 June 1996.

REMOTE SENS. ENVIRON. 59:167–179 (1997)

655 Avenue of the Americas, New York, NY 10010

0034-4257/97/$17.00
PII S0034-4257(96)00150-2

tation over large regions (Tucker et al., 1984; Malingreau and Tucker, 1988; Nelson and Holben, 1986; Nelson et al., 1987; Skole and Tucker, 1993). Although initial regional estimates diverged widely, they converged in recent years as a result of a wider utilization of high-resolution (<100 m) sensors (Townshend and Justice, 1988; Skole et al., 1994; Moran et al., 1994). Deforestation has been quantified with the use of Landsat Thematic Mapping (TM) imagery over the entire legal Amazon (Skole and Tucker, 1993) and in southeast Asia through NASA's Landsat Pathfinder (LP) project (Chomentowski et al., 1994). Forest, clearings, and secondary growth are well separated spectrally. Yet, several problems remain. First, the various stages of secondary regrowth are not easily differentiated. Second, cloud cover is a ubiquitous problem in the humid tropics, which limits deforestation assessments in time and space. Third, optical sensors are not good tools for measuring stand characteristics such as density and biomass (Sader et al., 1989). As a result, deforestation assessments are conducted over periods of several years, ground coverage is not complete, and information on woody biomass and the accumulation rate of secondary growth is limited and site specific.

Carbon models often do not include the role of secondary forests, because it is not well known what fraction of the landscape they occupy, how much carbon they accumulate and how quickly, and what fraction of secondary forests is subsequently recleared. Secondary forests have lower stocks of carbon, but they accumulate carbon quickly in the 10–20 years after disturbances if the site is not degraded (Uhl et al., 1988; Brown and Lugo, 1990).

Separating different ages of regrowth is possible with multiyear optical data (Lucas et al., 1993; Moran et al., 1994; Adams et al., 1995; Steininger, 1996), but performing this task over the entire Amazon basin would be daunting. These multiyear techniques are site specific, are limited by the availability of cloud-free images, and provide little information on woody biomass.

One alternative is to combine single-date optical data with radar data. Imaging radars can acquire continental-scale data sets without being constrained by cloud cover, thereby allowing more frequent and systematic assessments of deforestation. The Japanese JERS-1 imaging radar mapped the entire Amazon basin in fall of 1995 and is planned to map the entire tropical biome in 1996 (Rosenqvist, 1996). In addition to their all-weather capability, imaging radars can provide information on woody biomass, forest structure, and understory vegetation because radar signals probe the larger-size constituents of the forest, such as branches and trunks, and penetrate deep into the forest canopy (Sader, 1987; Dobson et al., 1992; Rignot et al., 1995).

The data collected in 1994 by NASA's Spaceborne Imaging Radar C (SIR-C) during its two missions were by far the most comprehensive data set of multichannel radar observations ever collected in the tropics. Its overflight of South America provided the first synoptic views of the Amazon basin at both C- (5.6 cm) and L-band (24 cm) frequency, with multiple polarizations, over regions long surveyed by optical sensors.

Our study site is located in the state of Rondonia, Brazil, within an area selected for intensive studies of tropical deforestation for the LP project and along a track for which fully polarimetric radar data were collected. The availability of full polarimetry is an important advantage over single- or dual-channel data because it provides a complete characterization of radar scattering at a given radar wavelength. It is then possible to analyze separately the contributions from surface scattering, volume scattering, or double bouncing of the radar signals. This analysis helps in turn to interpret the type of geophysical information obtainable from the radar data, resolve uncertainties in interpretation of single- or dual-channel data, and predict the performance level of existing and future imaging radars.

The objectives of this study were to develop an understanding of the mode of interactions of multichannel radar signals with deforested terrain in the tropics, determine the performance of Spaceborne Imaging Radar C (SIR-C) and Landsat TM at mapping various stages of forest degradation and regrowth, and study the possible synergy between the two instruments and the prospects for future combined use of both technologies. To validate the results, we employed a Landsat TM classification from 1993, a nine-year time series of SPOT XS imagery utilized to determine the age of clearings and land-use history, and a field visit conducted in October 1995.

STUDY SITE

The study site is located 50 km southeast of Porto Velho, the capital of the state of Rondonia, in a region of low relief, with gently rolling topography, high precipitation, and tropical seasonal climate (Kauffman et al., 1995). Deforestation has increased in Rondonia at a very high rate in the past two decades (Malingreau and Tucker, 1988). Colonization and agricultural expansion programs started in 1968 and accelerated in 1984 with the completion of highway BR-364, which facilitated immigration into Rondonia. The region once supported a continuous cover of primary tropical moist rain forest. About 12 percent of the Rondonia forests were cleared in the 1980s (Skole et al., 1994), where there was little deforestation in the 1970s. Most clearings are established by felling and burning of the forest, mostly by families (Dale et al., 1993). Much of the land is now in pasture of various quality for cattle and in secondary growth of various ages. Smaller plots are planted with coffee, maize, beans, and other crops. Unproductive fields are quickly abandoned, typically after 3–4 years, returning to forest regrowth (Alves and Skole, 1996). Regrowth is typically vigorous and dominated by several pioneer species,

Table 1. Data Sets Used in This Study

Sensor	*Type*	*Pixel Spacing*	*Date*	*Channels*	*Incidence Angle*
SIR-C	Radar	12.5 m	06-10-94	C- and L- quad-pol	37
JERS-1	Radar	12.5 m	23-10-95; 02-94	L-band HH	39
Landsat TM	Optical	30 m	07-10-93	7 bands	NA
SPOT XS	Optical	20 m	07/08-86/94	3 bands	NA

mostly *Cecropia spp.* and *Vismia gulanensis*, which yield a regular and homogeneous canopy structure.

REMOTE SENSING DATA

The data set utilized in this study is described in Table 1. The SIR-C data were acquired along a single track named Manaus CSAP-B, Brazil, at 02:18 A.M. local time during orbit 94 of the space shuttle *Endeavour*. The data were fully calibrated in the Jet Propulsion Laboratory (JPL) SIR-C processor. The false-color composite image shown in Fig. 1 is centered a 8°58′ S, 63°17′ W. The SIR-C data were spatially registered to a Landsat TM scene after rotation and resampling (cubic interpolation) of the radar imagery to a 30-m pixel spacing on the ground, using 28 tie-points between the two scenes. The rms error in registration is less than one image pixel.

One cloud-free Landsat TM scene was acquired on 7 October 1993 at 30-m spatial resolution. Areas of nonforest appear blue in Fig. 2, secondary growth is red, and primary forest has an intermediate, darker red signature.

One JERS-1 radar scene was acquired on 10 February 1994, during the wet season (Fig. 3a), and another was acquired on 23 October 1995, during the dry season (Fig. 3b). JERS-1 operates an L-band, horizontally polarized radar from an orbital altitude of 570 km, with an illumination angle of 39 degrees from the vertical (Table 1). The 1995 image was available at high resolution, 12.5-m pixel spacing, which we reduced to 25 m by spatial averaging. The 1994 scene was available only at 100-m pixel spacing, with a poorer radiometric fidelity. Both images were referenced to the same Landsat TM scene, using tie-points.

Multispectral SPOT XS data from 1986, 1988, 1989, 1991, 1992, and 1994 (no good data were available for 1987 and 1990) were available at a 20-m spatial resolution. SPOT XS has green visible, red visible, and near-infrared channels, but no midinfrared channel equivalent to that available on Landsat TM. All SPOT XS data were acquired in July and August.

Comparing the July SPOT 1994 with the October SIR-C 1994, we found many areas cleared in October that were not yet cleared in July, suggesting that new clearings in the July-August SPOT scenes could actually be from the previous dry season. This observation is consistent with Fearnside (1990), who states that September is the most popular month for felling trees in Amazonia.

FIELD SURVEY

We visited the test site in late-October 1995, one year after the SIR-C flight. Forest clearings that occurred in the previous months were easily identified on the ground because of the fire scars (Fig. 4d). Visiting the area with satellite imagery in hand and a preliminary analysis of the data helped optimize the field selection, the type of observations to be made, and the positioning and navigation from one field to the next. Ground photographs were taken in all four directions in the 24 emplacements we visited (Fig. 4). For each site, we noted the Geographic Positioning System (GPS) location, major types of land cover [pasture (Fig. 4c), forest, forest regrowth (Fig. 4a), slash-and-burn (Fig. 4b), etc.] and, whenever possible, estimated the approximate age of clearings (same year, previous year, or older).

METHODS

The SPOT XS images were analyzed visually to estimate the age of clearings and the history of land use since 1986. Only four categories of land cover were used: water, forest, nonforest, and secondary growth. Those categories were combined between the different years to determine the dynamics of land use. We limited the analysis to only three categories: (1) nonforest areas in the 1994 scene that showed no vegetation regrowth since the date of initial clearing between 1986 and 1992; (2) clearings from 1986, 1988, or 1989 that showed steady vegetation regrowth and no reclearing until 1994; and (3) clearings from 1991, 1992, or 1993 that showed steady vegetation regrowth and no reclearing until 1994. Category 1 defines clearings with no residual woody biomass. Category 2 defines intermediate regrowth 5–8 years of age. Category 3 defines initial regrowth 0–4 years of age. In this manner, we identified 66 test areas of known type of land cover.

The classification technique used for the Landsat TM data was an iterative self-organizing data analysis technique (Tou and Gonzalez, 1974) to define the inherent spectral clusters (40 clusters) within the data. A convergence threshold of 95% was used with only three iterations required to meet this threshold. A minimum distance classifier was applied to assign the pixels to the clusters. A human interpreter familiar with the spectral characteristics of the main classes of land cover then as-

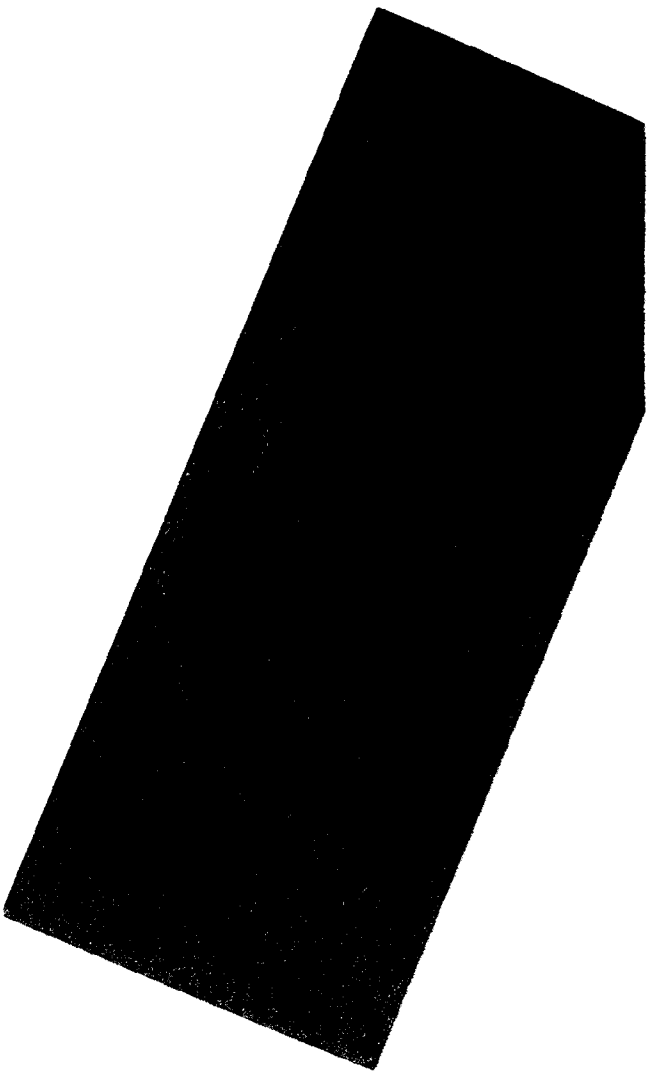

Figure 1. False-color composite image of the area imaged by SIR-C in Rondonia, Brazil, on 7 October 1994. L-band HH is red, L-band HV is green, and C-band HV is blue. North is at the top. Image size is 20.7 km by 25 km. Pixel spacing is 12.5 m, and spatial resolution is 25 m on the ground in both along-track (azimuth) and across-track (range) direction. SIR-C illuminated the scene from the right, at an altitude of 213 km, with an incidence angle at scene center of 37°. Red is the radar amplitude measured at L-band frequency (24 cm) HH-polarization (horizontal receive and transmit); green is L-band HV-polarization (horizontal receive and vertical transmit); and blue is C-band (5.66 cm) frequency, HV-polarization.

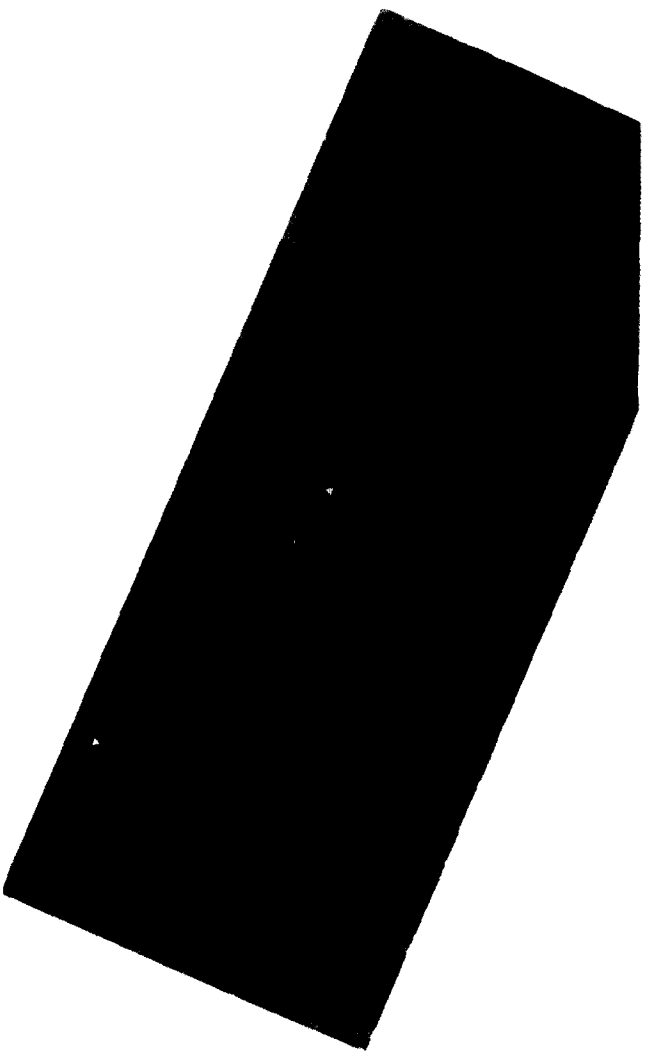

Figure 2. False-color composite image of the test site imaged by Landsat TM on 7 October 1993. Band 4 (near-infrared) is red, band 3 (red visible) is green, and band 5 (midinfrared) is blue.

signed the output clusters to our thematic classes of water, forest, nonforest, and secondary growth (Fig. 5).

The SIR-C data were classified by using a supervised procedure. One or two training areas were selected among the various types of land cover visually separated in the false-color composite SIR-C image. Increasing the number of training areas did not increase classification accuracy and also lowered the number of sites utilizable for independent testing of the classification accuracy. Labeling of the training sites into land-cover types was based on: (1) the results of the Landsat TM classification (forest versus nonforest); (2) the results of the field visit; and (3) a knowledge of radar scattering from vegetated terrain. The last means, for example, that areas of lowest radar backscatter at cross polarization were assumed to correspond to areas with no woody biomass, whereas areas showing the brightest response at horizontal polarization were assumed to include significant wood debris on the forest floor or to be flooded. The land-cover categories separated by SIR-C were: (1) open water; (2) flooded dead forest; (3) nonforest with no woody biomass; (4) initial regrowth of low biomass; (5) clearings with slash of high woody biomass; and (6) primary forest (Table 2). A maximum a posteriori Bayesian classifier (Rignot and Chellappa, 1992) was utilized to classify the entire scene into those six classes (Fig. 6). This classifier

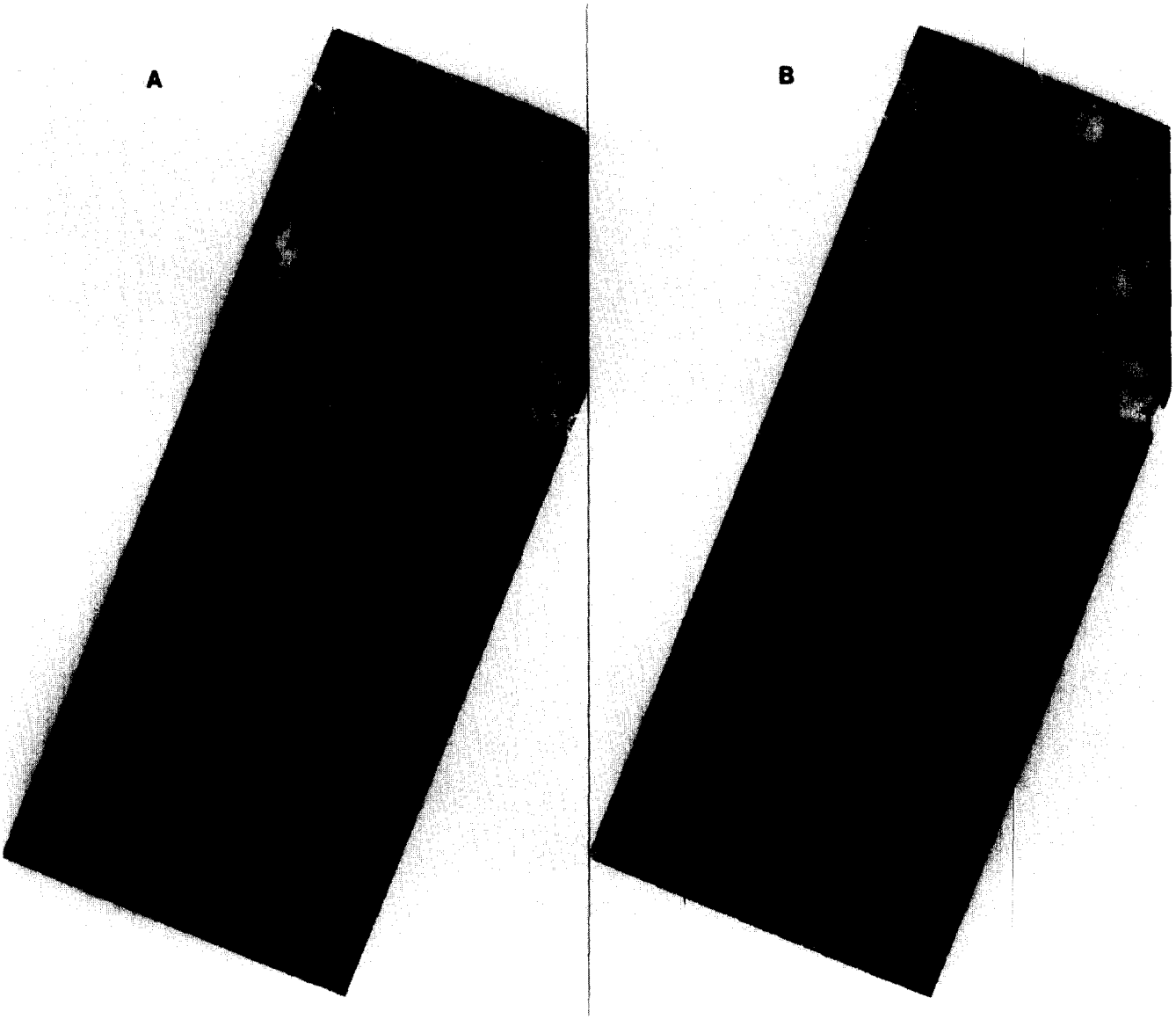

Figure 3. JERS-1 radar images of the test site acquired on (a) 23 October 1995; (b) 10 February 1994. ©NASDA.

is superior to a maximum likelihood classifier because it includes contextual information to estimate the a priori probabilities of the classes.

To help understand the radar scattering properties of the scene, we utilized a mathematical decomposition of the SIR-C polarimetric signal into three canonic forms of scattering named (1) single-bounce scattering; (2) double-bounce scattering, and (3) volume scattering (van Zyl, 1992). Single-bounce scattering (blue in Fig. 7) corresponds to single reflections of the radar signals on the reflecting surface. Double bouncing (red) corresponds to double reflections, and volume scattering (green) corresponds to multiple scattering interactions. The intensity of each color is proportional to the contribution of each canonic form of scattering to total backscatter. The decomposition does not provide information on the type of land cover present on the ground, because it is merely a mathematical decomposition of the signal, but the results help in the scientific analysis of the data.

RESULTS AND DISCUSSION

Analysis of Radar Scattering

At both L- and C-band, volume scattering dominates (Fig. 7). In the decomposition, the amount of volume scattering is determined by the intensity of the cross-polarized returns (van Zyl, 1992), which, according to scattering models of forested canopies, is controlled by the volume, the structure, and the moisture content of the canopy (Durden et al., 1989; van Zyl, 1989). The vegetation green component is larger at L- than at C-band. The interpretation is that the canopy is dense enough at C-band to result in single reflections from the canopy

Figure 4. Examples of land-cover types at test site in November 1995: (a) 1993 clearing with regrowth from 1989 in the background and one-year-old regrowth in foreground (Area 4a in Fig. 2); (b) 1993 clearing misclassified as nonforest by Landsat (Area 4b in Fig. 2); (c) pasture misclassified as secondary growth by Landsat (Area 4c in Fig. 2); (d) 1995 clearing (Area 4d in Fig. 2).

(blue); whereas, at L-band, the signals penetrate deeper and interact more with the canopy volume (green).

In the flooded forests bordering the Rio Jamari, double bouncing dominates (red). Most of these trees were killed by permanent river flooding in 1989 after the completion of Samuel Dam. The lower part of the trunks above the water level is probably rotten and moist because of continuous exposure to the river waters and seasonal flooding. We attribute their strong radar brightness to double reflections of the radar signals on the reflectors formed by the wet part of the dead trunks and the flooded ground. Owing to the absence of live canopy, as indicated by the Landsat TM data, volume scattering is limited and penetration into the canopy is enhanced, which facilitates double-bounce interactions. Surface scattering is weak because the radar signals bounce off the highly reflective flooded ground away from the radar looking direction.

In old clearings, single bouncing (blue) dominates, suggesting scattering from the ground layers. The proportion of volume scattering increases slightly at C-band compared with L-band, which is attributed to the greater interaction of the C-band signals with the short vegetation (grasses and shrubs).

Recently cleared areas behave differently from any other types of land cover. Double bouncing, single bouncing, and volume scattering contribute almost equally to total backscatter, resulting in a nearly white tone in Figure 7, especially at L-band. Double bouncing of the radar signals on the remaining standing trunks is therefore not the dominant source of backscatter (Stone and Woodwell, 1988). Double bouncing is less pronounced than in flooded areas because the forest floor is less reflective of the radar illumination. Volume scattering is still significant because the forest includes much wood debris and many standing live trees (Fig. 4b). Strong single-bounce scattering is likely due to the presence of felled tree trunks. Radar scattering from a layer

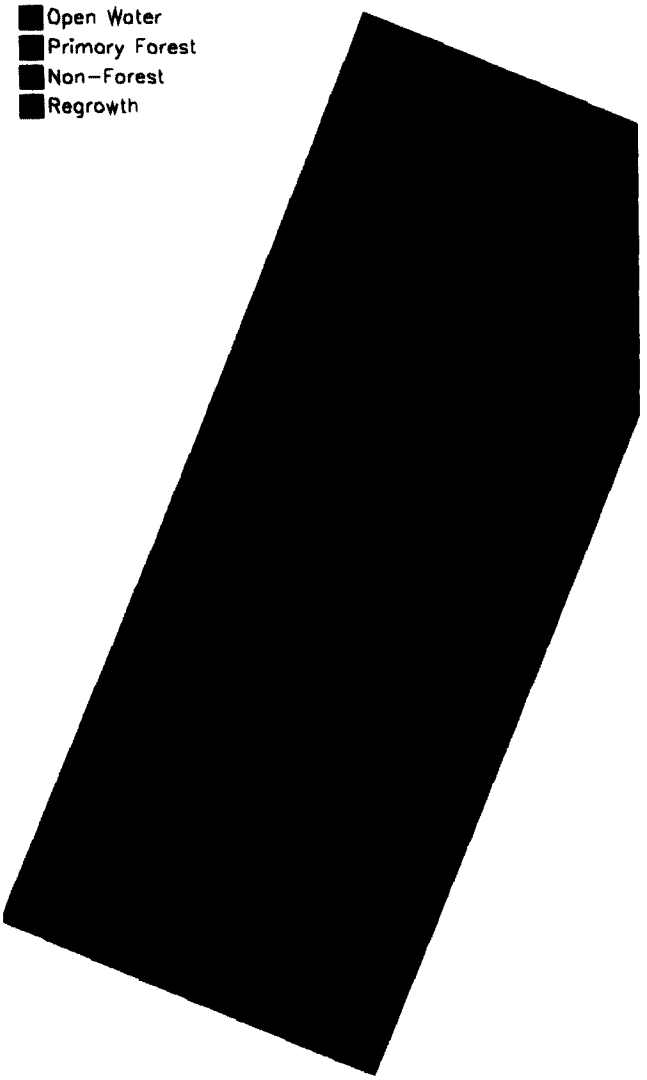

Figure 5. Classification map of the Landsat TM 1993 data.

of randomly oriented, horizontal, dielectric cylinders can be significant, if not dominant, at horizontal polarization (Rignot, 1995).

SIR-C and Landsat TM Land-Cover Mapping

We examined the accuracy of the SIR-C and Landsat TM classifications, using the 66 test areas. Each area was drawn as a polygon on the computer, and each pixel was used to report the classification results into confusion matrices (Table 3). A kappa coefficient of agreement was computed for each class (Rosenfield and Fitzpatrick-Lins, 1986). A combined kappa coefficient for the entire classification was calculated by dividing the sum of the numerators of the kappa coefficients computed for each class by the sum of their denominators, and not as the average of the kappa coefficients for each class.

Open water has low optical radiance and low radar backscatter (Table 2) and is mapped with high accuracy (Table 3). The Landsat TM data map small river streams in the midst of primary forest better than SIR-C, which confuses the streams with forest because of edge effects (trees bordering the streams yield high radar returns from trunk-ground reflections, whereas the radar returns from the water itself are low). A few pixels of very low backscatter in old clearings are misclassified as water by SIR-C.

Flooded dead forests are distinctly radar-bright, with large (120 degrees) phase difference between HH- and VV-polarized returns at both C- and L-band (Table 2). These forests could not be separated from open water in the Landsat TM data, because they have no live biomass, and are not included in Table 3b. Separating flooded dead forests from other types of disturbed forests is, however, relevant because their destruction did not result from logging activities.

With Landsat TM, nonforests are defined as bright in bands 3 and 5 and correspond on the ground to pasture, bare fields, and clearings with slash of high woody biomass. With SIR-C, nonforests are defined as areas of no woody biomass, meaning low HH- and HV-polarized returns at L-band (Table 2), and correspond on the ground to pastures, bare fields, or small areas of subsistence cultivation. The classification accuracy of Landsat TM data (Table 3b) is lower than that obtained with SIR-C data (Table 3c) because several nonforest areas are misclassified as regrowth areas. One example is shown in Fig. 4c.

Forest is mapped accurately with the Landsat TM data because its spectral characteristics are very distinct from all other classes of land cover (Fig. 3). In the SIR-C data, primary forest has the highest L-band cross-polarized backscatter, indicative of high crown biomass, and an intermediate level of brightness at the other polarizations, suggesting no preferred orientation and distribution of scatterers of slashed forests (Table 2). Textural variations in radar backscatter are large in the forest (Table 2), indicating a heterogeneous ground cover. Without using texture, forest is mapped accurately with SIR-C (Table 3c). Most errors are errors of commission where intermediate regrowth and 1-year-old slash and burn areas are misclassified as forest.

Less-than-1-year-old clearings with slash of high woody biomass are mapped accurately with SIR-C, but only three sites are available for testing (Table 3c). Those sites exhibit a very bright horizontal-polarized response. Not all 1994 clearings exhibit similar radar characteristics. For instance, several 1994 clearings close to highway BR-364 show low cross- and like-polarized returns, indicating no residual woody biomass and suggesting that most wood debris had been burned or removed by the time SIR-C imaged the site. Similarly, other 1994 clearings are classified as initial regrowth by SIR-C because their radar response is lower than that of other recent clearings, indicating lower residual biomass.

One-year-old clearings are not well separated from

Table 2. Radar Characteristics of Eight Training Areas Used to Classify the SIR-C Data

Band	σ°_{HH}	σ°_{HV}	σ°_{VV}	ρ_{HHVV}	φ_{HHVV}	*Land-Cover Type*
L-						
	−19.5	−29.8	−18.3	0.42	−5	Open water
	−10.6	−20.8	−11.0	0.55	10	Clearings with no woody biomass
	−9.2	−18.9	−11.0	0.46	10	Clearings with no woody biomass
	−4.4	−17.7	−9.0	0.40	−120	Flooded dead forest
	−5.8	−15.8	−8.3	0.38	−5	Initial Regrowth
	−6.0	−13.9	−8.2	0.31	−15	Initial Regrowth
	−5.2	−13.9	−7.4	0.40	−5	Slash of high woody biomass
	−7.4	−12.1	−7.4	0.29	0	Primary forest
C-						
	−16.4	−24.1	−16.7	0.27	−15	Open water
	−3.9	−11.9	−5.8	0.46	0	Clearings with no woody biomass
	−4.8	−11.6	−5.5	0.46	0	Clearings with no woody biomass
	−1.8	−17.1	−7.7	0.35	−130	Flooded dead forest
	−3.2	−13.3	−5.3	0.54	0	Initial Regrowth
	−4.0	−10.4	−4.6	0.42	−5	Initial Regrowth
	−3.2	−11.2	−4.4	0.49	−5	Slash of high woody biomass
	−4.7	−10.5	−4.7	0.46	0	Primary forest

σ°_{HV} is the radar backscatter expressed in dB at HV-polarization. ρ_{HHVV} is the normalized correlation coefficient between the HH- and VV-polarized radar returns. φ_{HHVV} is the phase difference in degrees between the HH- and VV-polarized radar returns.

the forest in the SIR-C data. Clearings that are initially brighter than the surrounding forest because they include slash of high woody biomass therefore decrease in radar brightness with time. Several hypotheses could explain the decrease in radar brightness. One is that woody biomass decreases with time because of reburning of the stand, but this effect could be small because most biomass burning usually occurs during the first season. A second effect is that vegetation regrowth progressively masks out the radar returns from the ground, but 1-year regrowth should not attenuate the L-band signals significantly. A third hypothesis is that the dead trunks lose their moisture over the years, lowering their dielectric constant and hence their reflectivity to radar signals. Further research is needed to determine which process has the most significant effect on radar backscatter.

With Landsat TM, secondary growth is defined as bright in band 4, moderate to bright in band 5, and of low reflectance in band 3. Crops have a moderate to high reflectance in band 5, but low reflectance in band 4. Few crops are present in our study area. Most of the cleared land is pasture. The Landsat TM data classify regrowth with 77% accuracy, because regrowth is often detected among old clearings (Table 3b and Fig. 4c). A portion of these clearings may have been abandoned in 1992, given the high rates of land abandonment in the area (Alves and Skole, 1996), so our accuracy estimates may underestimate the performance of the Landsat TM classification.

With SIR-C, secondary regrowth is defined as an intermediate level of cross-polarized brightness between nonforest and forest, with no preferred vertical or horizontal structure compared with recent clearings with slash. Forest regrowth is mapped with 69% accuracy (Table 3c). Most errors correspond to intermediate regrowth 5–8 years of age being misclassified as forest. Earlier studies conducted with airborne imaging radars on monospecie forests have shown that L-band single-polarization data saturate at about 100 tons/ha woody biomass (Sader, 1987). Total above-ground woody biomass of secondary forests was measured to range from 44 to 120 tons/ha in this area (Kauffman et al., 1995), with a rate of regrowth of about 12 to 16 tons/ha/yr for first time regrowth (Kauffman, personal communication, 1996). Hence, the woody biomass of intermediate regrowth is likely close to the 100 tons/ha limitation of the L-band radar technique. Landsat TM imagery separates young secondary forest from primary forest better because primary forests contain many different tree species of variable canopy structure.

Vegetation regrowth older than 9 years was not included in the discussion because we found only a few stands already in some stage of regrowth in the SPOT XS 1986 that were left undisturbed thereafter. The largest one of them, probably older than 10 years in 1994, was no longer separated from the forest in the SPOT 1989 data.

SIR-C and Landsat TM Synergy

The foregoing results suggest the Landsat TM data separate deforested areas from the forest better than the SIR-C data because the SIR-C data do not separate older regrowth from the forest well. On the other hand, the SIR-C data provide better information on the residual woody biomass of deforested terrain.

We combined the two classifications by using logical

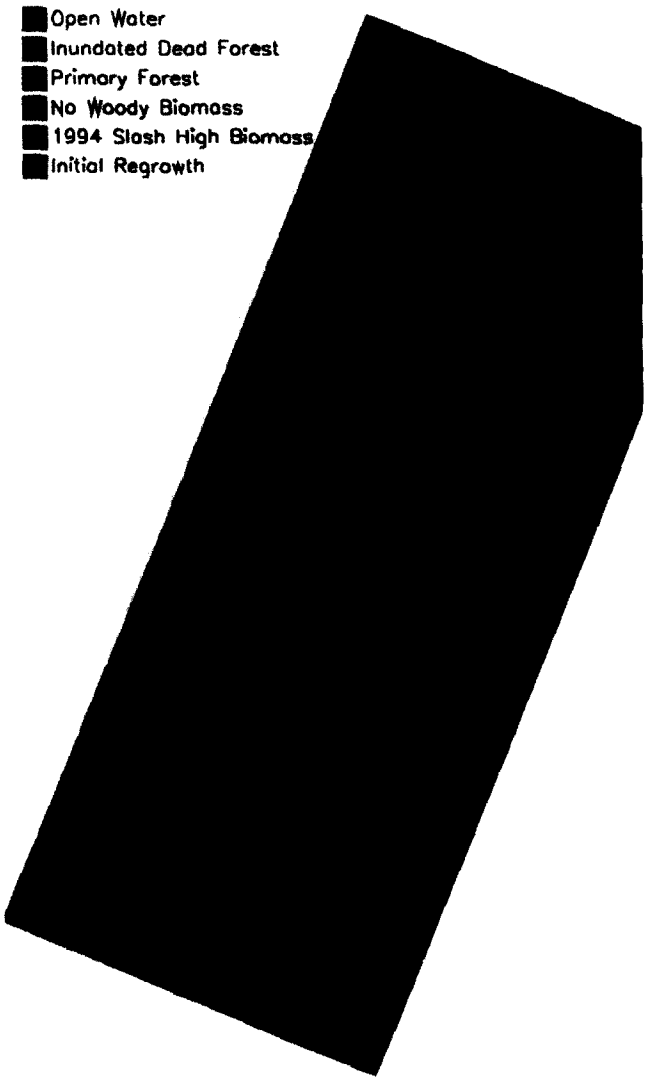

Figure 6. Classification map of the SIR-C 1994 data.

operators to define seven classes of land cover: (1) open water; (2) flooded dead forest; (3) nonforest with no woody biomass; (4) initial regrowth; (5) intermediate regrowth; (6) recent clearings with slash of high woody biomass; and (7) forest. Forests were mapped by using only the Landsat TM classification. Flooded dead forests, nonforest, and initial regrowth were mapped by using only the SIR-C classification. Open water was mapped by using the Landsat TM classification, excluding flooded forests mapped by using the SIR-C data. Recent clearings with slash of high woody biomass included those identified in the SIR-C classification alone, plus areas classified as clearings in the Landsat TM imagery and forest in the SIR-C imagery that corresponded to 1993 clearings. Intermediate regrowth combined areas classified as forest by SIR-C and as regrowth by Landsat TM.

The radar-optical combination (Fig. 8) results in a net increase in classification accuracy (Table 3a). Not shown in Table 3a is the classification accuracy of initial and intermediate regrowth combined, which is 92%, a 20% gain compared with using SIR-C alone. All seven classes are now separated with high accuracy.

Discussion

The final results permit a more reliable assessment of the areal extent of various types of land cover. Intact forests occupied 67% of the landscape in 1994, still the dominant land-cover type in 1994. The deforestation rate is 1.7% for 1994. This value is higher but consistent with the 1.5 percent estimate calculated by Alves and Skole (1996) in 1992 over a larger area.

Deforested areas occupy 27% of the total area, the rest being open water and flooded dead forests. Of the 27%, 17% are clearings with slash of high woody biomass, 35% are clearings with no residual biomass, and 47% are in some stage of regrowth, mostly initial regrowth. Intermediate regrowth comprises only 5% of the deforested areas. Hence, forest regrowth is an important form of land use—almost half of the deforested areas—but most of it is young. This means that secondary growth is recleared quickly, typically after 4–5 years. This result is consistent with the study of Alves and Skole (1996).

Clearings from 1994 (classified as forest in the Landsat TM classification and nonforest in the SIR-C classification) were classified as clearings with slash of high residual woody biomass (31%), initial regrowth (52%), and clearings with no residual biomass (17%). These numbers suggest that residual woody biomass is highly variable among new clearings. To characterize this spatial variability at the large scale, satellite radar imagery could clearly be an essential complement to field studies.

Recent measurements conducted near the town of Jamari (Kauffman et al., 1995) provide useful indications of the range of biomasses encountered in the area. Total biomass consumption for slash-and-burn sites ranges from 42% to 57%, corresponding to residual total aboveground biomasses ranging from 140 to 220 tons/ha. For comparison, the biomass of primary forest ranges from 292 to 436 tons/ha. For initial regrowth (with the use of a regrowth rate of 12 to 16 tons/ha/yr valid for first-time regrowth), woody biomass probably ranges from several tons per hectare to about 60 tons/ha. For intermediate regrowth, woody biomass probably ranges from 60 to 120 tons/ha. The various classes of land cover used in our classification therefore correspond to very different levels of woody biomass. At the same time, woody biomass varies significantly within each class. This land-cover classification is therefore not sufficiently detailed to provide accurate biomass inputs for carbon models. Quantitative estimates of woody biomass must be obtained from the radar data for each class of land cover. To convert the radar data into biomass numbers, we need to examine in more detail the relation between the radar signals and

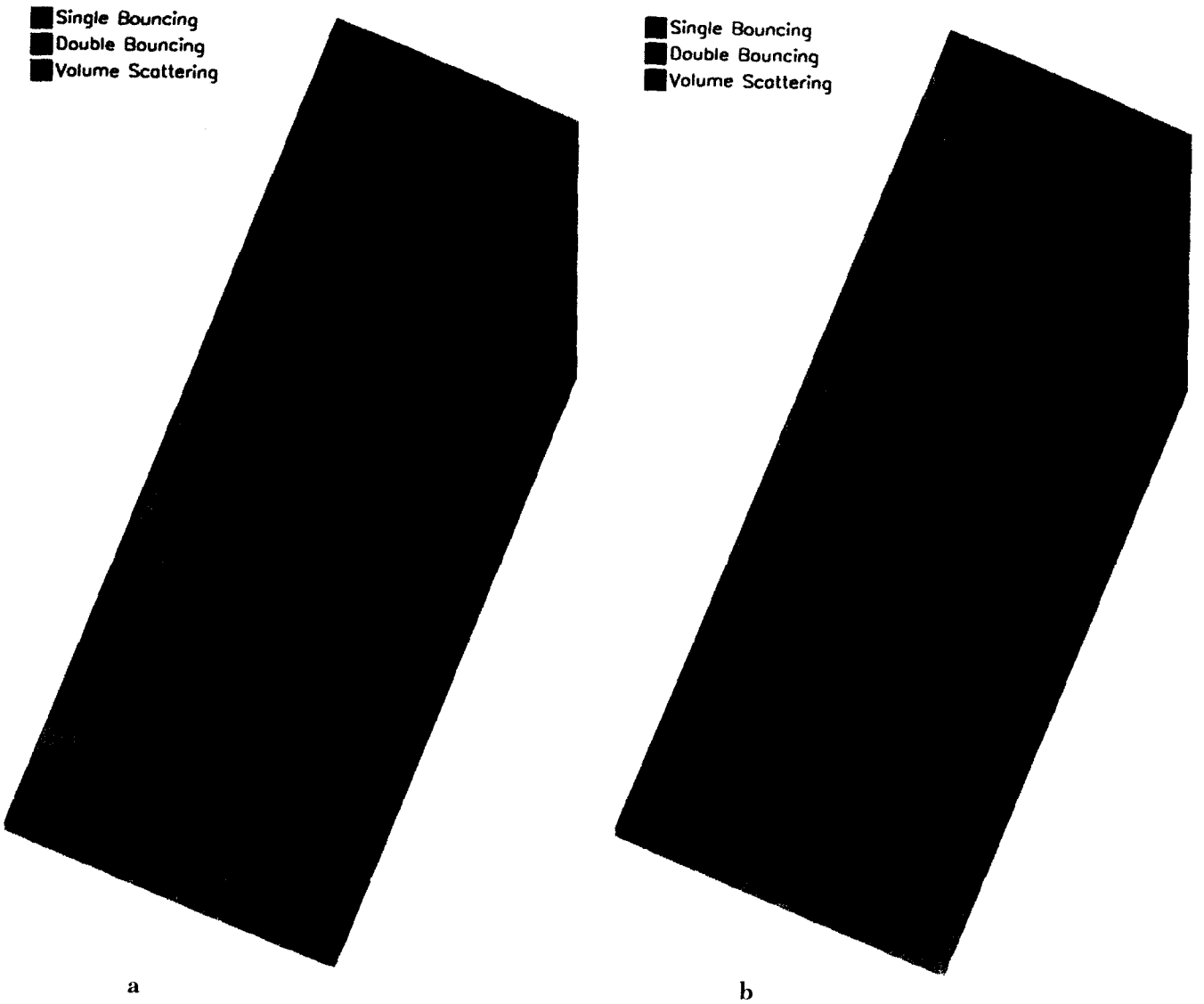

Figure 7. Mathematical decomposition of the polarimetric signal at (a) C-band and (b) L-band frequencies into double-bounce scattering (red), volume scattering (green), and single-bounce scattering (blue).

the biomass numbers obtained from field studies. This type of work is the focus of our ongoing studies. The results will be reported in the future.

Potential of International Imaging Radars

C-band VV data from SIR-C do not separate forest from recent slash (Table 2) and provide only a 2–3 dB contrast between forest and pasture (Table 2), compared with more than 6 dB at L-band (Table 2). C-band HH data yield brighter returns in recent slash of high biomass, and nonforest is better separated from the forest than at C-band VV, but other types of land cover are poorly separated from the forest. With single-date imagery, C-band radars of the class of the European Remote Sensing 1 (ERS-1) and the Canadian Radarsat imaging radars should have limited potential for deforestation studies.

L-band HH-polarized data are a priori more appropriate for detecting changes in woody biomass. Over our Rondonia test site, JERS-1 radar data acquired in 1994 during the rainy season (Fig. 4a) underestimate deforestation by more than 100% because forest fallow and undisturbed forests have similar brightnesses. Recent clearings are slightly brighter than the forest, but the contrast is less than that with the SIR-C data. Data acquired in 1995 during the dry season (Fig. 4b) show a better contrast between intact forest and deforested areas, but most areas of regrowth are not well separated from forest, and 1995 clearings are not easily distinguishable.

Comparing the mapping accuracy obtained by using SIR-C data at various polarizations and frequencies (Table 3d), we find that at least two polarizations are required at L-band, preferably HH and HV, to separate regrowth with good accuracy. Polarimetric information eventually provides the highest mapping accuracy, espe-

Table 3. Classification Accuracy in Percent of the SIR-C and Landsat TM Data into OW, Open Water; FDF, Flooded Dead Forest; CC, Clearings with No Woody Biomass; INIR, Initial Regrowth; INTR, Intermediate Regrowth; S, Recent Clearings with Slash of High Woody Biomass; and F, Forest.

(a) SIR-C+Landsat TM
Number of Sites: 66=OW (2), FDF (4), CC (33), INIR (10), INTR (12), S (3), F (2)
Number of Pixels Tested: 45225.
Combined Kappa Coefficient: 93

	OW	*FDF*	*CC*	*INIR*	*INTR*	*S*	*F*	*Kappa*
OW	227	0	0	0	0	0	0	100
FDF	153	5525	0	30	2	34	12	95
CC	86	0	14640	138	17	30	46	97
INIR	1	0	17	6451	864	339	131	79
INTR	0	0	0	205	922	28	196	67
S	0	0	0	111	0	3458	35	96
F	5	0	0	0	0	0	11524	100

(b) Landsat TM
Number of Sites: 51 (no 1994 clearings, no flooded forest)=OW (2), CC (26), INIR (22), F (2)
Number of Pixels Tested: 28690
Combined Kappa Coefficient: 83

	OW	*CC*	*INIR*	*F*	*Kappa*
OW	160	0	0	0	100
CC	0	9575	2138	80	70
INIR	0	144	1991	329	77
F	0	0	0	11061	100

(c) SIR-C L-band quad C-band quad
Number of Sites: 66=OW (2), FDF (4), CC (33), INIR (22), S (3), F (2)
Number of Pixels Tested: 45225
Combined Kappa Coefficient: 91

	OW	*FDF*	*CC*	*INIR*	*S*	*F*	*Kappa*
OW	198	0	25	2	0	2	87
FDF	0	5525	0	54	160	15	95
CC	78	0	14648	138	13	80	97
INIR	0	0	17	6656	1	2480	68
S	0	0	0	111	3451	42	95
F	0	0	0	0	0	11529	100

(d) Kappa Coefficients for Various SIR-C Combinations

Class	*L-Quad, C-Quad*	*L-Quad*	*L-HH,HV/ C-HH,HV*	*L-HH,VV*	*L-HH,HV*	*L-HH*
OW	87	66	86	63	64	63
FDF	95	86	68	92	30	8
CC	97	92	97	92	93	92
INIR	68	64	57	42	61	14
SB	95	94	94	95	86	77
F	100	100	100	100	100	100
Combined	91	87	84	82	76	58

Kappa is the kappa coefficient calculated either for each class or for the entire classification (combined). Each row of the confusion matrix shows the number of pixels classified in the categories listed in the columns.

cially for regrowth. C-band data help only to separate open water and flooded forests. The classification accuracy of L-band HH data is 20% lower than that achieved by using two polarizations and is low for areas of regrowth.

These results confirm that single-channel systems will have difficulties at mapping deforestation on a single date. With multidate imagery, the conclusions may be different. Change-detection techniques have led to some of the most powerful applications of the ERS-1 radar instrument for land-cover mapping applications. It is therefore still very important to examine the usefulness of

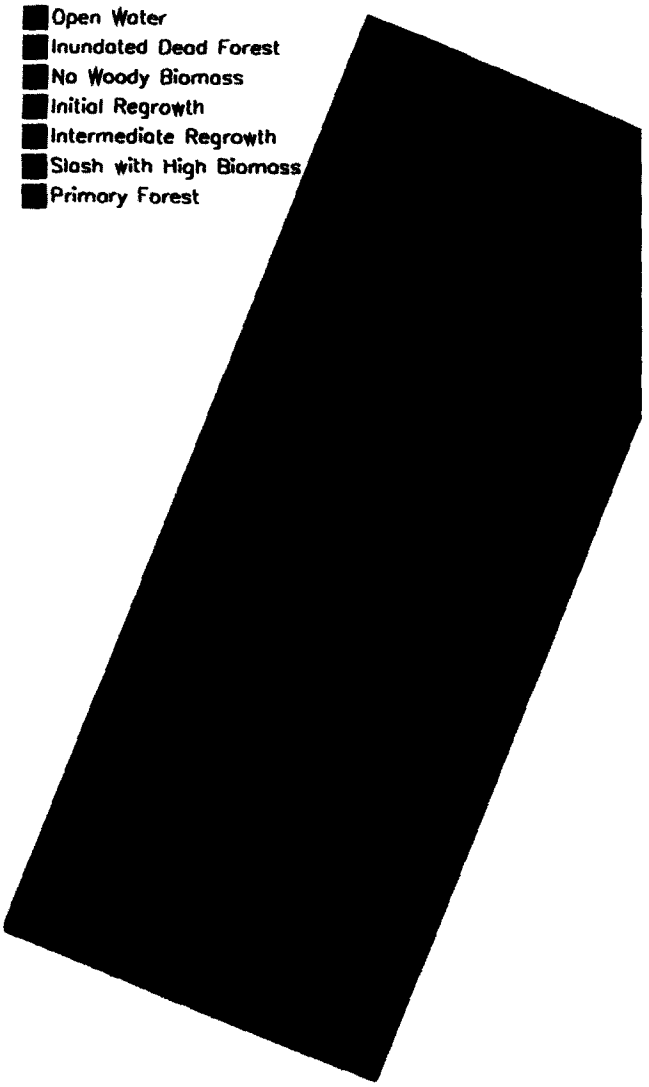

Figure 8. Classification map combining the SIR-C and Landsat TM classifications.

multidate JERS-1 data, preferably acquired during the dry season, to detect deforestation and forest regrowth in the tropics by using change-detection techniques.

CONCLUSIONS

Comparing the classification performance of SIR-C and Landsat TM in a test site in Rondonia, Brazil, we find that the Landsat TM data map the extent of deforested areas very well and better than the SIR-C data; but, in deforested areas, the SIR-C data provide more useful information on residual woody biomass levels. Intermediate regrowth is not well separated from the forest in the SIR-C data, but this form of land use occupies a small fraction of the landscape because of the high rate of reclearing of secondary growth. Imaging radars operating at the longer radar wavelengths could overcome this limitation because their signals tend to saturate at higher biomass levels (Dobson et al., 1992) and successional forest is better separated from primary forest (Rignot et al., 1995). The combined use of optical and radar imagery eventually provides the most reliable form of land-cover mapping, without necessarily requiring data from the same year. Future studies need to examine the potential of multidate imagery from the existing spaceborne imaging radars in more detail, and need to combine the radar data with in situ measurements of woody biomass to provide quantitative inputs to carbon models over large areas.

This work was partly carried out at the Jet Propulsion Laboratory, California Institute of Technology, under a contract with the National Aeronautics and Space Administration. The authors would like to thank Walter Chomentowski for assistance in the field survey; the Landsat Pathfinder project and the IGBP-DIS high resolution data exchange pilot project for providing the Landsat and SPOT data; NASDA for providing the JERS-1 images of Rondonia and ASF/JPL for processing it; and the JPL people who processed, calibrated, and distributed the SIR-C images.

REFERENCES

Adams, J. B., Sabol, D. E., Kapos, V., Filho, R. A., Roberts, D. A., Smith, M. O., and Gillespie, A. R. (1995), Classification of multispectral images based on fractions of end-members: applications to land-cover change in the Brazilian Amazon. *Remote Sens. Environ.* 52:137–154.

Alves, D. S., and Skole, D. L. (1996), Characterizing land cover dynamics using multi-temporal imagery. *Int. J. Remote Sens.* 17:835–839.

Brown, S., and Lugo, A. E. (1990), Tropical secondary forests. *J. Trop. Ecol.* 6:1–32.

Chomentowski, W. H., Salas, W. A., and Skole, D. L. (1994), Landsat Pathfinder project advances deforestation mapping. *GIS World* 7:34–38.

Dale, V. H., O'Neill, R. V., Pedlowski, M., and Southworth, F. (1993), Causes and effects of land-use change in central Rondonia, Brazil. *Photogramm. Eng. Remote Sens.* 59:997–1005.

Dobson, M. C., Ulaby, F. T., LeToan, T., Beadoin, A., Kasischke, E. S., and Christensen, N. (1992), Dependence of radar backscatter on conifer forest biomass. *IEEE Trans. Geosci. Remote Sens.* 30:412–415.

Durden, S. L., van Zyl, J. J., and Zebker, H. A. (1989), Modeling and observation of the radar polarization signature of forested areas. *IEEE Trans. Geosci. Remote Sens.* 27:290–301.

Fearnside, P. M. (1990), Fire in the tropical rain forest of the amazon basin, in *Fire in the Tropical Biota: Ecological Studies, 84*, (J. G. Goldammir, Ed.), Springer-Verlag, pp. 106–116.

Houghton, R. A. (1991), Tropical deforestation and atmospheric carbon cycle. *Clim. Change* 19:99–118.

Houghton, R. A., and Skole, D. L. (1990), Carbon, in *The Earth as Transformed by Human Action* (B. L. Turner et

al., eds.), Cambridge University Press, Cambridge, U.K. pp. 393–408.

Houghton, R. A., Skole, D. L., and Lefkowitz, D. S. (1991), Changes in the landscape of Latin America between 1850 and 1985, II: a net release of CO_2 into the atmosphere. *J. Forest Ecol. Mgmt.* 38:133–199.

Kauffman, J. B., Cummings, D. L., Ward, D. E., and Babbit, R. (1995), Fire in the Brazilian Amazon, 1: biomass, nutrient pools, and losses in slashed primary forests. *Oecologia* 104:397–408.

Lucas, R. M., Honzak, M., Foody, G. M., Curran, P. J., and Corves, C. (1993), Characterizing tropical secondary forests using multi-temporal Landsat sensor imagery. *Int. J. Remote Sens.* 4:3061–3067.

Malingreau, J. P., and Tucker, C. J. (1988), Large-scale deforestation in the southeastern Amazon basin of Brazil. *Ambio* 17:49–55.

Moran, E. F., Brondizio, E., Mausel, P., and Wu, Y. (1994), Integrating Amazonian vegetation, land-use, and satellite data. *Bioscience* 44:329–338.

Neftel, A., Moor, E., Oeschger, H., and Stauffer, B. (1985), Evidence from polar ice cores for the increase in atmospheric CO_2 in the past two centuries. *Nature* 315:45–47.

Nelson, R., and Holben, B. (1986), Identifying deforestation in Brazil using multiresolution satellite data. *Int. J. Remote Sens.* 7:429–448.

Nelson, R., Horning, N., and Stone, T. A. (1987), Determining the rate of forest conversion in Mato-grosso, Brazil, using Landsat MSS and AVHRR data. *Int. J. Remote Sens.* 8:1767–1784.

Rignot, E. (1995), A model for interpreting the unusual radar echoes from the Greenland Ice Sheet. *J. Geophys. Res.* 100:9389–9400.

Rignot, E., and Chellappa, R. (1992), Segmentation of polarimetric synthetic aperture radar data. *IEEE Trans. Imag. Proc.* 1:281–300.

Rignot, E., Zimmerman, R., van Zyl, J. J., and Oren, R. (1995), Spaceborne applications of a P-band imaging radar for mapping of forest biomass. *IEEE Trans. Geosci. Remote Sens.* 33:1162–1169.

Rosenfield, G. H., and Fitzpatrick-Lins, K. (1986), A coefficient of agreement as a measure of thematic classification accuracy. *Photogramm. Eng. Remote Sens.* 52:223–227.

Rosenqvist, A. (1996), The global rain forest mapping project by JERS-1 SAR. *XVIII ISPRS Congress in Vienna, Austria*, July 9–19, in press.

Sader, S. A. (1987), Forest biomass, canopy structure, and species composition relationships with multipolarization L-band synthetic aperture radar data. *Photogramm. Eng. Remote Sens.* 53:193–202.

Sader, S. A., Waide, R. B., Lawrence, W. T., and Joyce, A. T. (1989), Tropical forest biomass and successional age class relationships to a vegetation index derived from Landsat TM data. *Remote Sens. Environ.* 28:143–156.

Skole, D. L., Chomentowski, W. H., Salas, W. A., and Nobre, A. D. (1994), Physical and human dimensions of deforestation in Amazonia. *Bioscience* 44:314–321.

Skole, D. L., and Tucker, C. J. (1993), Tropical deforestation and habitat fragmentation in the Amazon: satellite data from 1978 to 1988. *Science* 260:1905–1910.

Steininger, M. K. (1996), Tropical secondary forest regrowth in the Amazon: age, area and change estimation with Thematic Mapper data. *Int. J. Remote Sens.* 17:9–27.

Stone, T. A., and Woodwell, G. M. (1988), Shuttle imaging radar A analysis of land use in Amazonia. *Int. J. Remote Sens.* 9:95–105.

Tou, J. T., and Gonzalez, R. C. (1974), *Pattern Recognition Principles*, Addison-Wesley, Reading, MA.

Townshend, J. R. G., and Justice, C. O. (1988), Selecting the spatial resolution of satellite sensors required for global monitoring of land transformations. *Int. J. Remote Sens.* 9:187–236.

Tucker, C. J., Holben, B. N., and Goff, T. E. (1984), Intensive forest clearing in Rondonia, Brazil, as detected by satellite remote sensing. *Remote Sens. Environ.* 15:255–261.

Uhl, C., Buschbacher, R., and Serrao, E. A. S. (1988), Abandoned pastures in eastern Amazonia, I: patterns of plan succession. *J. Ecol.* 76:663–681.

van Zyl, J. J. (1989), Unsupervised classification of scattering behavior using radar polarimetry data. *IEEE Trans. Geosc. Remote Sens.* 27:36–45.

van Zyl, J. J. (1992), Application of Cloude's target decomposition theorem to polarimetric imaging radar data. *Proc. SPIE* 1748:184–191.